STRUCTURAL AND MORPHOLOGICAL CHARACTERIZATION OF ERBIUM DOPED HYDROXYAPATITE FOR MEDICAL IMAGING

Andrei Viorel PADURARU[1,2], Adina Magdalena MUSUC[1,3], Ovidiu Cristian OPREA[1,2,4], Roxana TRUSCA[1,2], Vasile-Adrian SURDU[1,2], Bogdan Stefan VASILE[1,2,5] , Ecaterina ANDRONESCU[1,2,5]

Luminescent erbium-doped hydroxyapatite nanomaterials were obtained by simple co-precipitation method at low temperature. The objective of this research was to study the influence of erbium ions on the morphology, structure and photoluminescent properties of hydroxyapatite. The synthesized powders were characterized by ICP-MS, FTIR spectrometry, UV-Vis spectroscopy, XRD diffraction and SEM analysis. These Er-dopped Hydroxyapatite materials demonstrated superior efficiency and can be used as luminescent labeling materials.

Keywords: Erbium, Hydroxyapatite, medical imaging

1. Introduction

Nowadays, diagnosis and imaging have a key role in the healthcare sector, and in this case all processes that involves detection, screening and image-guided smart nanomedicine are expected to be further developed. To obtain photoluminescence (PL) imaging, conventional contrast agents – such as organic dyes [1], metal complexes [2], proteins with fluorescent properties, and modified silica [3] must be used, with the condition that the compounds should follow the principle of Stokes-shift emissions [4]. A group of materials that has gain interest in the past decade is rare earth-doped optically active nanostructured materials with applications in imaging and therapy using drug delivery systems. Lanthanide coordination compounds have a high value of the Stokes shift and long lifetime of the excited state, making them a perfect material for bioimaging [5].

[1] Faculty of Applied Chemistry and Materials Science, Department of Science and Engineering of Oxide Materials and Nanomaterials, University POLITEHNICA of Bucharest, Romania, contact e-mail: andrei93.paduraru@yahoo.com
[2] National Centre for Micro and Nanomaterials, University POLITEHNICA of Bucharest, Bucharest, Romania
[3] "Ilie Murgulescu" Institute of Physical Chemistry, Romanian Academy, Bucharest, Romania
[4] National Research Centre for Food Safety, University POLITEHNICA of Bucharest, Romania
[5] Academy of Romanian Scientists, Bucharest, Romania.

Alumina (Al_2O_3), titania (TiO_2), zirconia (ZrO_2) and other oxides, calcium phosphates (CaPs) and bioactive glasses have made substantial contributions in the medical field [6]. Recently, hydroxyapatite (HA) with molecular formula: $Ca_{10}(PO_4)_6(OH)_2$ has been widely used as a contrast agent, in tissue engineering and drug delivery [7–9]. The crystal structure of HA is stoichiometrically composed of Ca and P ions and the cell unit has a unique hexagonal structure, suitable for the replacement of Ca^{2+} sites with lanthanide ions [10-11]. The Ca/P molar ratio for HA is 1.67 [12–13].

Many studies have shown that HA could be easily substituted by different ions, such as monovalent ions Na^+, K^+, divalent ions Zn^{2+}, Cu^{2+}, Mg^{2+}, trivalent ions Au^{3+}, Ag^{3+}, La^{3+} or tetravalent ions Ti^{4+}, Zr^{4+} [14-16]. Depending on the properties needed in the synthetized material – geometry, crystallinity, size, stoichiometry and degree of particle agglomeration, hydroxyapatite could be obtain using multiple methods and precursors. The main methods used to obtain hydroxyapatite are conventional method, wet chemical synthesis, hydrothermal conversion of calcium carbonate, bone calcination, solid phase reactions, coprecipitation, sol-gel method and biomimetic synthesis [17–28].

It is known that pure hydroxyapatite doesn't show florescence under visible excitation and Ca^{2+} ions do not possess luminescence but provide biodegradability. Rare earth elements have a surprising spectral nature, being successfully used as a non-isotropic substitute for organic fluorides. Applications of this group of elements range from *in vivo* detection of cell function and luminescent marking of molecules to clarification of the structure and functions of proteins and enzymes.

Over time, the existence of erbium ions (Er^{3+}) in bones (especially in the ribs) has been extensively studied and using this chemical element as substitution agent of hydroxyapatite shown an improvement in the biological properties of the material [29]. Many studies have demonstrated the optical and biological properties of erbium-doped hydroxyapatite and the possibility to use Er-HA in biomedical field with a molar ratio of (Ca + Er)/P of 1.59 – 1.72, a change in morphology and size due to the replacement of large Ca^{2+} ions (0.099 nm) with smaller Er^{3+} ions (0.088 nm) and a strong emission at about 1540 nm, due to a thermic treatment at 1100 °C – 1200 °C [29-31].

The main goal of this study is to demonstrate the application of the obtained erbium-doped hydroxyapatite by the co-precipitation method as fluorescent probing for cellular imaging. The present research analysis is conducted through the variation from 0 to 10% of erbium ion concentration, and in consequence its influence in structural and luminescence properties of the hydroxyapatite powders. Moreover, the differences and the influences of erbium ions on the crystalline structure, morphology, surface characteristics, and the photoluminescence properties were also investigated.

2. Synthesis of erbium-doped hydroxyapatite

Erbium-doped hydroxyapatite nanomaterials were synthesized by coprecipitation method using the same method developed in our previous studies [32-34]. Materials used for the synthesis: $Ca(NO_3)_2 \cdot 4H_2O$, erbium-(III) nitrate pentahydrate, ammonium phosphate dibasic, NH_4OH 25% solution and deionized water. Pure HA was synthesized using the same methodology, without the addition of erbium precursors.

3. Physical and chemical characterization

Inductively coupled plasma mass spectrometry (ICP-MS) was applied to determine the content of Er^{3+} in the mineral phase of the substituted hydroxyapatite.

Raman spectroscopy studies were performed, using a Horiba equipment with an excitation wavelength of 514 nm.

FTIR spectra were recorded with a Nicolet iS50R spectrometer, at room temperature, in the measurement range 4000–400 cm^{-1}, in ATR mode at 4 cm^{-1} resolution. The X-ray diffraction (XRD) spectra were recorded using a PANalytical Empyrean diffractometer at room temperature, with a Cu X-ray tube (λ Cu Kα1 = 1.541874 Å) operating in-line focusing, with programmable divergent slit on the incident side and a programmable anti-scatter slit mounted on the PIXcel3D detector on the diffracted side.

The SEM morphology of the studied samples was analyzed using a Quanta Inspect F50 FEG (field emission gun) scanning electron microscope with 1.2 nm resolution.

UV-Vis diffused reflectance spectra were obtained using a Able Jasco V560 spectrophotometer, with a scan speed of 200nm/s, between 200 and 850 nm. The fluorescence spectra were measured by using a Perkin Elmer LS 55 fluorescence spectrophotometer. Spectra were recorded with a scan speed of 200 nm/s between 350 and 800 nm, and with excitation and emission slits widths of 4, 7 and 10 nm, respectively. An excitation wavelength of 320 nm was used.

4. Results and Discussion

4.1. ICP-MS analysis

The erbium ions presented in doped HA were analyzed by ICP-MS technique. Table 1 shows the measured concentrations, the correlation coefficient and limit of detection for each ion concentration. The data confirms the presence of erbium ions in doped hydroxyapatite powders. It was found that the content of dopant increases from 0.5 to 10% in concordance with the used concentrations.

Table 1

Erbium ions contents for substituted HA

Sample	Element	µg element/ mg sample	Limit of detection (LoD) / [ug/l]	Correlation coefficient (r)
$Er_{0.5}HAp$	166Er	7.71	0.0016	0.998
$Er_{1}HAp$		13.38		
$Er_{2.5}HAp$		31.55		
$Er_{5}HAp$		62.11		
$Er_{10}HAp$		121.28		

4.2. FTIR analysis

FTIR spectra of Er_xHA samples are shown in Fig. 1. All absorption bands characteristic for HA and reported in literature [35] appear in the FTIR spectrum of pure HA. The FTIR spectrum of pure HA (black line from Fig. 1) shows a broad band in the region 3000 - 3400 cm^{-1} which corresponds to adsorbed water. The bands around 1090, 1023 and 960 cm^{-1} are due to the stretching mode of P-O [36]. The bands around 602 cm^{-1}, 562 cm^{-1} and 474 cm^{-1} are attributed to the bending mode of O-P-O [37]. The band at around 873 cm^{-1}, which appears in all studied compounds spectra, is due to the $[HPO_4]^{2-}$ ions [38-40].

Comparing the FTIR spectra from Fig. 1:

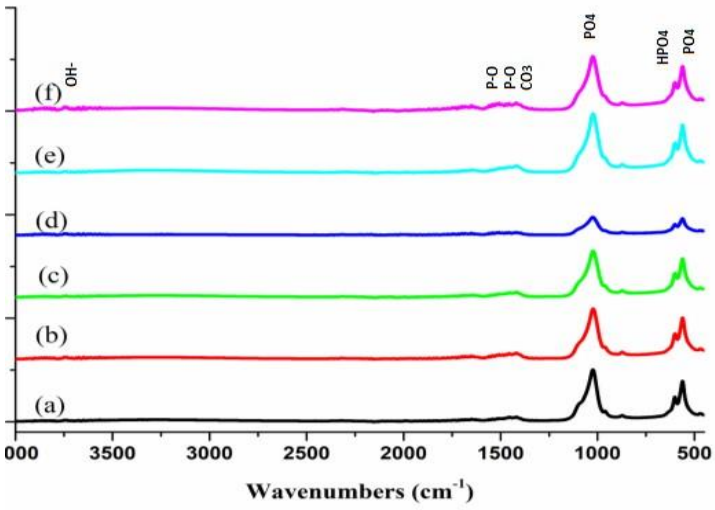

Fig. 1. FTIR spectra of pure HAp (a); $Er_{0.5}HAp$ (b); $Er_{1}HAp$ (c); $Er_{2.5}HAp$ (d) $Er_{5}HAp$ (e); $Er_{10}HAp$ (f).

it was found that the FTIR spectra of Er_xHA powders with various erbium concentrations are similar to pure HA. In all FTIR spectra of Er_xHA samples, the

absorption bands which appear around 873 and 1426 cm^{-1} are assigned to CO_3^{2-}. This can be attributed to the CO_3^{2-} groups that replaced the PO_4^{3-}groups, indicating a reaction between HA and carbon dioxide in the air [41]. The intensity of phosphate bands decreases with increase of erbium concentrations until the molar fraction of erbium is 0.25%. Above this concentration the banding bands of O-P-O increases. An explanation is that the replacement of calcium ions with erbium ions causes a change of bonding forces between the ions resulting a weakness of the banding bands of O-P-O [37]. The increasing in concentration of doping erbium ions resulted in a reduction of the intensity of the bands, associated with a decrease of HA crystallinity.

4.3. Raman spectroscopy

Raman spectra of the samples of hydroxyapatite doped with Erbium are presented in Fig. 2. All vibration bands characteristics of hydroxyapatite and reported in literature appears in the Raman spectra of pure HA. The peaks observed at 427.4–447.3 cm^{-1} are characteristic to ν_2 PO_4^{3-} ions (P-O stretching) and 576.7 – 608.2 cm^{-1} corresponds to bending of P-O bond from PO_4^{3-} (ν_4) group. The formation of pure HA is highlighted by the narrow peak at 960.3 cm^{-1}. The peak between 1025.6 and 1122.4 cm^{-1} are attributed to asymmetric stretch of P-O (PO_4^{3-} ν_3 group). By increasing the substitution degree, a reduction of the intensity of vibration bands can be observed. This can be correlated with XRD and FTIR results.

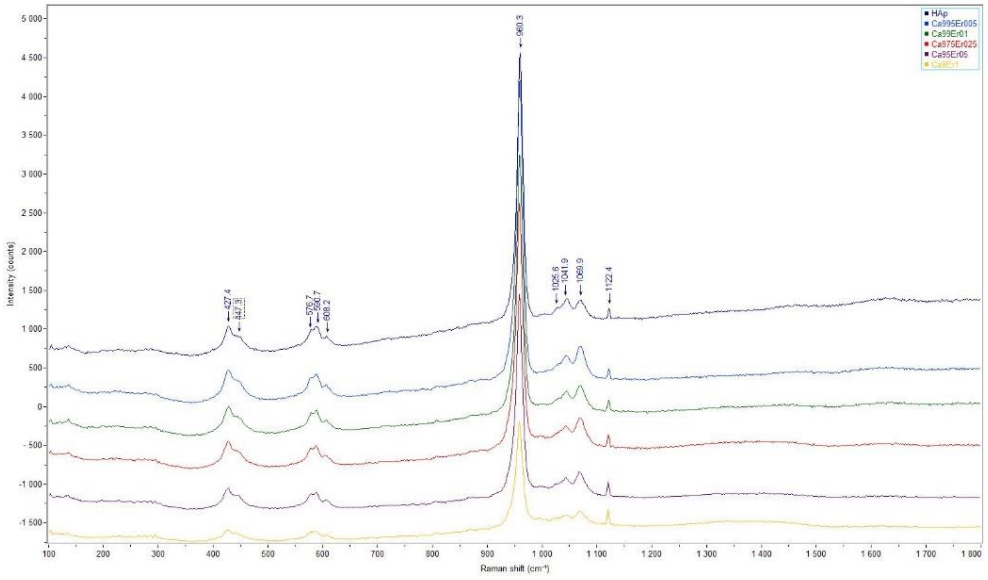

Fig. 2. Raman spectra of Erbium-doped hydroxyapatite

4.4. X-ray Diffraction

The XRD patterns of studied doped hydroxyapatite, with erbium ion with different concentration, and the pure HAp reveal the formation of a pure hexagonal HA phase (according to ICDD PDF4+ card no 00-068-0738, Fig. 2) [42], in agreement with literature [43-45]. The XRD patterns of all studied samples indicate only the pure hexagonal HA phase of the space group $P6_3/m$, with all diffraction peaks of HA standard JCPDS database (PDF4+ card no 00068-0738) such as: (002), (121), (112), (030), (022), (130), (222), (123) and (004).
The degree of crystallinity and the crystallite size of studied samples are shown in Table 2. In all studied samples, the intensities of X-ray peaks decrease with the ion doping concentration level increases, indicating an interference of rare earth ions with crystal structure of HA.

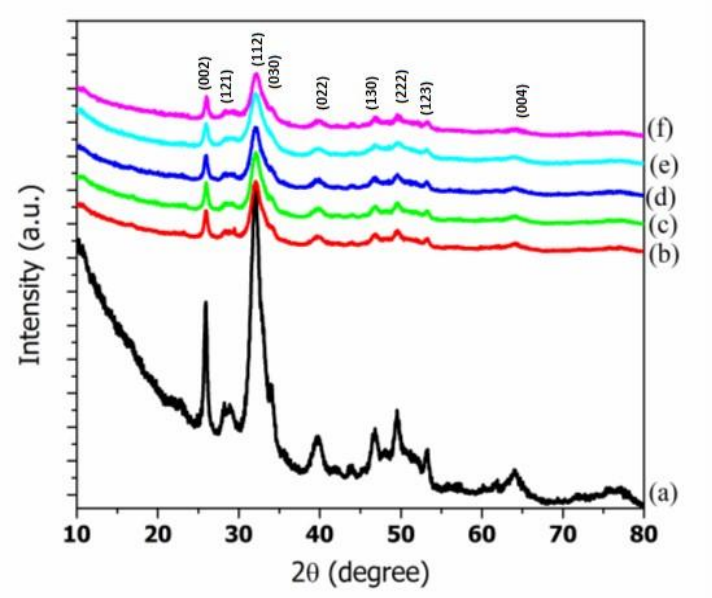

Fig. 3. X-ray diffraction patterns of pure HAp (a); $Er_{0.5}$HAp (b); Er_1HAp (c); $Er_{2.5}$HAp (d) Er_5HAp (e); Er_{10}HAp (f).

Table 2

Calculated crystallite size (D) values and degree of crystallinity (χ_c) of pure HA and different doped hydroxyapatite with various amount of erbium ions

Samples	D/ nm	S /%	χ_c / %
HAp	6.07±0.82	1.52±0.53	31.50
Er0.5HAp	5.71±0.65	1.62±0.58	37.53

Er1HAp	6.46±0.77	1.43±0.52	37.41
Er2.5HAp	5.33±0.57	1.73±0.65	36.02
Er5HAp	4.89±0.60	1.89±0.69	35.65
Er10HAp	4.74±0.39	1.96±0.80	32.74

The average crystallite size of the pure HA was of 6.07 nm and for the erbium ions-doped HA powders was observed a slowly decrease in crystallite size with increasing ion dopant content [46-48]. Analyzing the data from Table 2 can be highlighted that the introduction of Er^{3+} in HA lattice induces an increase of crystallite size from 5.71 to 6.46 nm and a decrease of microstain from 1.62% to 1.43%. Then, for a substitution degree of more than 2.5%, it was observed a decrease of crystallite size from 5.33 nm to 4.74 nm at 10% Er^{3+} substitution. The lattice microstrain increase to 1.96% in the case of maximum substitution degree.

4.5. SEM Analysis

The SEM morphologies of pure HA and erbium doped hydroxyapatite with various concentrations were shown in Figs. 4. The SEM image of pure HAp (Fig. 4a) reveals dense particles with spherical shape and size in the range of 5-9 nm.

By doping with erbium ion, a little influence can be observed in the morphology of substituted HA when it was compared with pure HAp.

SEM morphologies of erbium doped hydroxyapatite (Fig. 4b-4f) revealed an agglomerated spherical and near elongated morphologies with particles size in the range of 2-6 nm. From below images can be observed decreases in particle size with increasing of erbium ions concentrations.

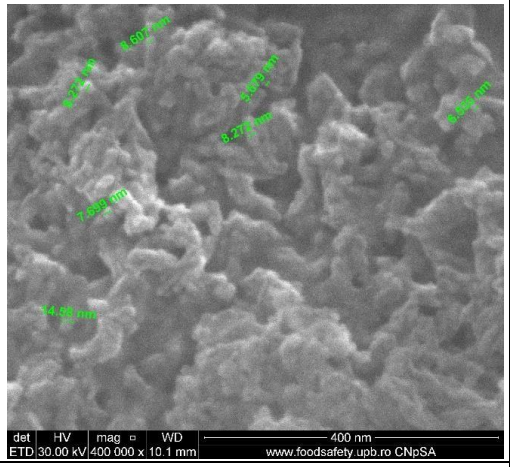

a

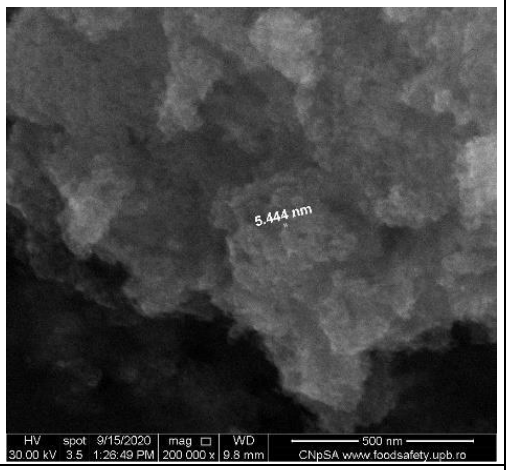

b

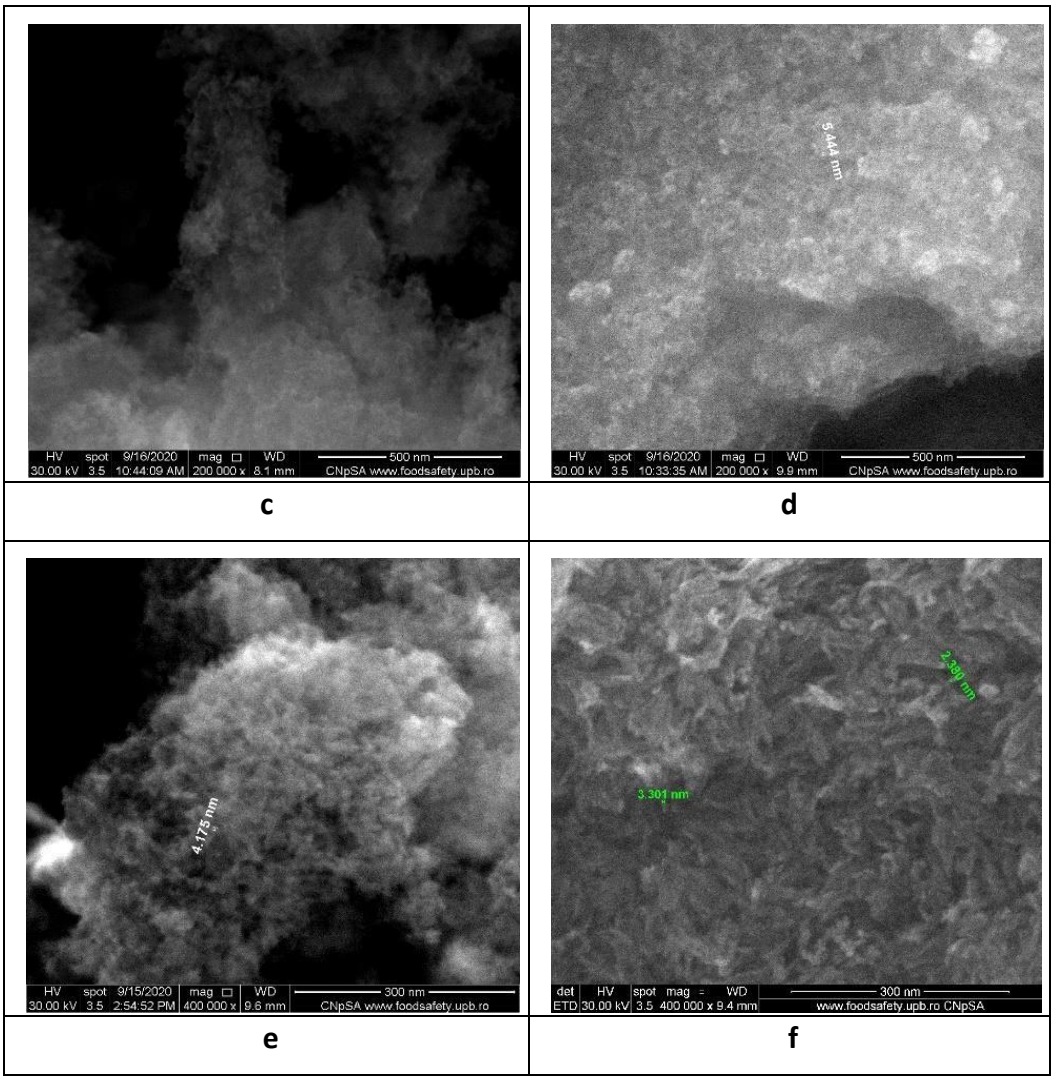

Fig. 4. The SEM images of pure Hap and Er_XHap (a) x=0 (b) x=0.5; (c) x=1; (d) x=2.5; (e) x=5; (f) x=10.

4.6. UV-Vis and PL Spectra

The UV-Vis spectra of all studied samples are shown in Fig. 5a. A general trend was observed for all studied compounds: an increase of intensity of absorption peaks and a broadening of them with increases of erbium concentrations in HA. The electronic spectra of erbium doped hydroxyapatite samples from Fig. 5a contain several bands, which increase in their intensities with increasing erbium concentration.

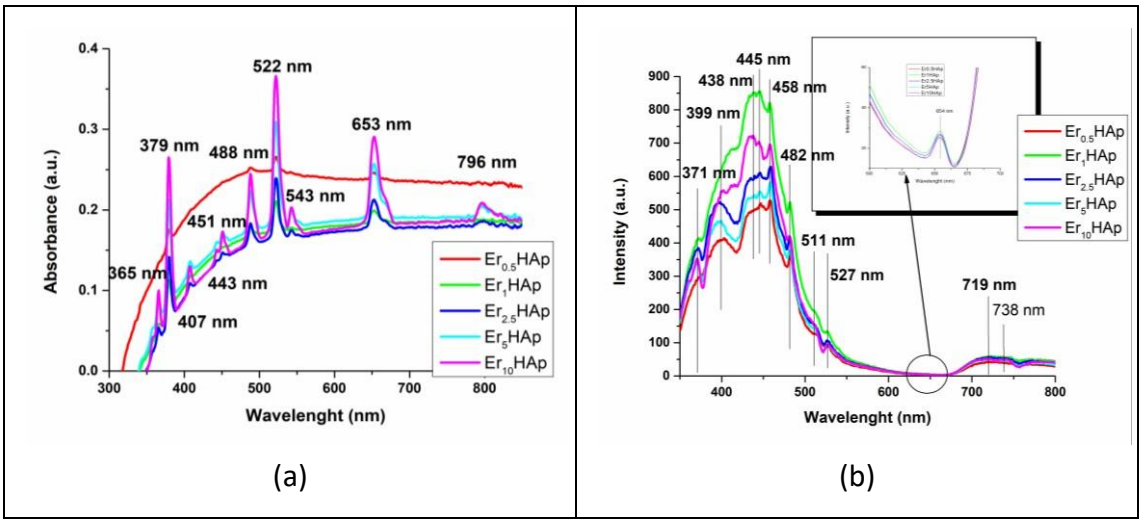

Fig 5. (a) UV-Vis absorption spectra of Er_xHA and (b) Room-temperature photoluminescence spectra of Er_xHA (inset - detailed Er_xHA), at different concentrations

The electronic spectrum of Er^{3+} shows several characteristic bands: at 379 nm assignable to $^1I_{15/2} \rightarrow {}^2G_{11/2}$ transition; at 407 nm assignable to $^4I_{15/2} \rightarrow (^2G,^4F,^2H)_{9/2}$ transition; at 443 nm assignable to $^4I_{15/2} \rightarrow {}^4F_{5/2}$; at 451 nm assignable to $^4I_{15/2} \rightarrow {}^4F_{3/2}$; at 488 nm assignable to $^4I_{15/2} \rightarrow {}^4F_{7/2}$; at 522 nm assignable to these peaks increase with increasing erbium content. The identified peaks on the electronic spectra of erbium doped hydroxyapatite could be ascribed to the 4f - 4f transition from ground state ($^4I_{15/2}$) to different energy states. The increase in erbium ions concentration leads to an increase in peak intensity may be due to the replacement of the Calcium ions with Erbium ions in the HAp structure.

The photoluminescence spectra of erbium doped hydroxyapatite are shown in Fig. 5b. The dominant emission spectrum of HAp presents in 350-530 nm domain an increase in intensities up to 0.1% erbium content, followed by a decreasing of bands intensities. The bands as a shoulder at 371 nm from $Er_{0.5}HAp$ samples becomes a clear band assigned to $^4I_{15/2}$ - $^4G_{11/2}$ transition. The band at 527 nm is superposed with $^2H_{11/2} - {}^4I_{15/2}$ transition of erbium ion, which increases in intensity with increasing erbium content, associated with various oxygen defects. Another three bands appear: at 371nm and 527 nm, assigned to $^4I_{15/2} \rightarrow {}^4G_{11/2}$ and $^4I_{15/2} \rightarrow {}^2H_{11/2}$ transitions and an emission band at 654 nm due to $^4I_{15/2}$ - $^4F_{9/2}$ transition (inset from Fig. 5b) [49,50].

6. Conclusions

This study presents the preparation of pure hydroxyapatite and Er-doped HAp, and thereafter the influence of doping ions on the formation and structure of

synthesized materials, using different concentrations of Erbium (0.05; 0.1; 0.25; 0.5 and 1).

For characterization of samples multiple physico-chemical techniques were used. Both FTIR spectroscopy and XRD diffraction analysis confirmed that erbium ions have replaced the calcium ions from HAp crystal lattice. It was observed that if the concentration of Er ions would increase over x = 0.5, there would be a decrease in hydroxyapatite crystallinity.

The SEM micrograph and TEM analysis were used to prove the morphology of pure HAp and Er-doped HAp. All studied samples presented a spherical morphology. The Er-doped HAp samples revealed strong florescent emission peaks, confirming that the photoluminescent properties were improved due to the use of Erbium ions.

REFERENCES

[1] Chen G, Qiu H, Prasad PN, Chen X. Upconversion nanoparticles: design, nanochemistry, and applications in theranostics. Chem Rev. 2014;114(10):5161214.

[2] B. Devika Chithrani, Arezou A. Ghazani, and Warren C. W. Chan, Determining the Size and Shape Dependence of Gold Nanoparticle Uptake into Mammalian Cells, Nano Lett. 2006, 6, 4, 662–668

[3] Liong M, Lu J, Kovochich M, Xia T, Ruehm SG, Nel AE, Tamanoi F, Zink JI. Multifunctional inorganic nanoparticles for imaging, targeting, and drug delivery. ACS Nano. 2008 May;2(5):889-96

[4] Mondal, S.; Park, S.; Choi, J.; Tran, L.H.; Yi, M.; Shin, J.H.; Lee, C.Y.; Oh, J. Bioactive, luminescent erbium-doped hydroxyapatite nanocrystals for biomedical applications. Ceram. Int. 2020, 46, 16020–16031.

[5] Andronescu, E.; Predoi, D.; Neacsu, I.A.; Paduraru, A.V.; Musuc, A.M.; Trusca, R.; Oprea, O.; Tanasa, E.; Vasile, O.R.; Nicoara, A.I.; Surdu, A.V.; Iordache, F.; Birca, A.C.; Iconaru, S.L.; Vasile, B.S. Photoluminescent Hydroxylapatite: Eu3+ Doping Effect on Biological Behaviour. Nanomaterials 2019, 9, 1187.

[6] Sergy V. Dorozhkin, and Umapada Pal, Recent progress on fabrication and drug delivery applications of nanostructured hydroxyapatite Sudip Mondal, WIREs Nanomed Nanobiotechnol 2017, e1504.

[7] Neacsu IA, Stoica AE, Vasile BS, Andronescu E. Luminescent Hydroxyapatite Doped with Rare Earth Elements for Biomedical Applications. Nanomaterials (Basel). 2019 Feb 10;9(2):239.

[8] Hyehyun Kim, Sudip Mondal, Subramaniyan Bharathiraja, Panchanathan Manivasagan, Madhappan Santha Moorthy and Junghwan Oh, Optimized Zndoped hydroxyapatite/Doxorubicin bioceramics system for efficient drug delivery and tissue engineering application, Ceramics International, 2018, 44(6), 60626071

[9] Sudip Mondal, Giang Hoang, Panchanathan Manivasagan, Madhappan Santha Moorthy, Thi Tuong Vy Phan, Hye Hyun Kim, Thanh Phuoc Nguyen and Junghwan

Oh, Rapid microwave-assisted synthesis of gold loaded hydroxyapatite collagen nano-biomaterials for drug delivery and tissue engineering application, Ceramics International, 2019, 45(3), 2977-2988,

[10] Dorozhkin SV, Epple M. Biological and medical significance of calcium phosphates. Angew Chem Int Ed Engl. 2002 Sep 2;41(17):3130-46. doi: 10.1002/1521-3773(20020902)41

[11] Rare earth element doped hydroxyapatite luminescent bioceramics contrast agent for enhanced biomedical imaging and therapeutic applications, Sudip Mondal, Van Tu Nguyen, Sumin Park, Jaeyeop Choi, Thi Mai Thien Vo, Joong Ho Shin, Yeon-Hee Kang, Jungh wan Oh, Ceramics International, 46, Issue 18, Part A, 2020, 29249-29260.

[12] Structure of biological apatite: bone and tooth, Ahmed Talal, Shorouq Khalid Hamid, Maria Khan, Abdul Samad Khan, in Handbook of Ionic Substituted Hydroxyapatites Woodhead Publishing Series in Biomaterials 2020, Pages 1-19

[13] Ion-doped hydroxyapatite: An impasse or the road to follow?, Vuk Uskoković, Ceramics International, 46, Issue 8, Part B, 2020, Pages 11443-11465

[14] Na-doped hydroxyapatite coating on carbon/carbon composites: Preparation, in vitro bioactivity and biocompatibility, Hejun Li, Xueni Zhao, Sheng Cao Kezhi Li, Mengdi Chen, Zhanwei Xu, Jinhua Lu, Leilei Zhang, Applied Surface Science 263, 2012, 163-173

[15] Charifa Boucetta, Mohamed Kacimi, Alain Ensuque, Jean-Yves Piquemal, Francois Bozon-Verduraz, Mahfoud Ziyad, Oxidative dehydrogenation of propane over chromium-loaded calciumhydroxyapatite, Applied Catalysis A: General 356 (2009) 201–210.

[16] J. Huang, S.M. Best, W. Bonfield, Tom Buckland, Development and characterization of titanium-containing hydroxyapatite for medical applications, Acta Biomaterialia 6 (2010) 241–249

[17] Mehdi Sadat-Shojai, Mohammad-Taghi Khorasani, Ehsan Dinpanah-Khoshdargi, Ahmad Jamshidi, Synthesis methods for nanosized hydroxyapatite in diverse structures, Acta Biomaterialia, 9, Issue 8, 2013, 7591-7621.

[18] J.Indira, K.S.Malathi, Comparison of template mediated ultrasonic and microwave irradiation method on the synthesis of hydroxyapatite nanoparticles for biomedical applications, Materials Today: Proceedings 51, Part 4, 2022, Pages 1765-1769.

[19] Yingkai Liu, Dedong Hou, Guanghou Wang, A simple wet chemical synthesis and characterization of hydroxyapatite nanorods, Materials Chemistry and Physics 86 (2004) 69–73.

[20] Ripamonti U. The morphogenesis of bone in replicas of porous hydroxyapatite obtained from conversion of calcium carbonate exoskeletons of coral. The Journal of Bone and Joint surgery. American Volume. 1991 Jun;73(5):692-703.

[21] Development of high strength hydroxyapatite by solid-state-sintering process, Sumit Pramanik, Avinash Kumar Agarwal, K.N. Rai, Ashish Garg, Ceramics International 33 (2007) 419–426.

[22] Vuong-Hung Pham, Hoang Nhu Van, Phuong Dinh Tam, Hanh Nguyen Thi Ha, A novel 1540 nm light emission from erbium doped hydroxyapatite/ βtricalcium phosphate through co-precipitation method, Materials Letters 167 (2016) 145–147.

[23] I. Mobasherpour, M. Soulati Heshajin, A. Kazemzadeh, M. Zakeri, Synthesis of nanocrystalline hydroxyapatite by using precipitation method, Journal of Alloys and Compounds 430 (2007) 330–333.

[24] Bose, S.; Saha, S.K. Synthesis of hydroxyapatite nanopowders via sucrosetemplated Sol-Gel method. J. Am. Ceram. Soc. 2003, 86, 1055–1057.

[25] Basam A.E. Ben-Arfa, Isabel M. Miranda Salvado, José M.F. Ferreira, Robert C. Pullar, Novel route for rapid sol-gel synthesis of hydroxyapatite, avoiding ageing and using fast drying with a 50-fold to 200-fold reduction in process time, Materials Science and Engineering C 70 (2017) 796–804.

[26] R.I.M. Asri, W.S.W. Harun, M.A. Hassan, S.A.C. Ghani, Z. Buyong, A Review of Hydroxyapatite-based Coating Techniques: Sol-gel and Electrochemical Depositions on Biocompatible Metals, Journal of the Mechanical Behavior of Biomedical Materials, 57, 2016, Pages 95-108.

[27] S. Türk, İ. Altınsoy, G. ÇelebiEfe, M. Ipek, M. Özacar, C. Bindal, Microwave–assisted biomimetic synthesis of hydroxyapatite using different sources of calcium, Materials Science and Engineering C 76 (2017) 528–535.

[28] Changmin Hu, Mark Aindow, Mei Wei, Focused ion beam sectioning studies of biomimetic hydroxyapatite coatings on Ti-6Al-4V substrates, Surface & Coatings Technology 313 (2017) 255–262.

[29] Ammar Z. Alshemary, Muhammed Akrama Yi-Fan Goh, Mohammed Rafiq Abdul Kadir, Ahmad Abdolahi, Rafaqat Hussain, Structural characterization, optical properties and in vitro bioactivity of mesoporous erbium-doped hydroxyapatite, Journal of Alloys and Compounds, 645, 2015, 478-486.

[30] Sudip Mondal, Van Tu Nguyen, Sumin Park, Jaeyeop Choi, Le Hai Tran, Myunggi Yi, Joong Ho Shin, Chang-Yong Lee, Junghwan Oh, Bioactive, luminescent erbium-doped hydroxyapatite nanocrystals for biomedical applications, Ceramics International, 46, 10, Part B, 2020, 16020-16031.

[31] Vuong-Hung Pham, Hoang Nhu Van, Phuong Dinh Tam, Hanh Nguyen Thi Ha, A novel 1540 nm light emission from erbium doped hydroxyapatite/ βtricalcium phosphate through co-precipitation method, Materials Letters 167 (2016) 145–147.

[32] Paduraru, A.V.; Oprea, O.; Musuc, A.M.; Vasile, B.S.; Iordache, F.; Andronescu, E. Influence of Terbium Ions and Their Concentration on the Photoluminescence Properties of Hydroxyapatite for Biomedical Applications. Nanomaterials 2021, 11, 2442.

[33] Paduraru, A.V.; Musuc, A.M.; Oprea, O.C.; Trusca, R.; Iordache, F.; Vasile, B.S.; Andronescu, E. Synthesis and Characterization of Photoluminescent Ce(III) and Ce(IV) Substituted Hydroxyapatite Nanomaterials by Co-Precipitation Method: Cytotoxicity and Biocompatibility Evaluation. Nanomaterials 2021, 11, 1911.

[34] AV Paduraru, O Oprea, AM Musuc, BS Vasile, A Ficai, E Andronescu, Photoluminescent nanomaterials based on europium doped hydroxyapatite, Roum. J. Mater. 2021 51 (3), 353-360.

[35] Vivek Dhand, K.Y. Rhee, Soo-Jin Park, The facile and low temperature synthesis of nanophase hydroxyapatite crystals using wet chemistry, Mater. Sci. Eng. C 36 (2014) 152-159.

[36] Qiuhua Yuan*, Caoping Qin, Jianbo Wu, Anping Xu, Ziqiang Zhang, Junquan Liao, Songxin Lin, Xiangzhong Ren, Peixin Zhang, Synthesis and characterization of Cerium-doped hydroxyapatite/ polylactic acid composite coatings on metal substrates, Materials Chemistry and Physics 182 (2016) 365-371

[37] Zude Feng, Yingmin Liao, Meng Ye, Synthesis and structure of cerium-substituted hydroxyapatite, Journal of Materials Science: materials in medicine 16 (2005) 417–421.

[38] H. Li, X. Sun, Y. Li, B. Li, C. Liang, and H. Wang, "Materials Science & Engineering C Preparation and properties of carbon nanotube (Fe)/ hydroxyapatite composite as magnetic targeted drug delivery carrier," Mater. Sci. Eng. C, vol. 97, no. December 2017, pp. 222–229, 2019.

[39] S. Mondal, A. Dey, U. Pal, Low temperature wet-chemical synthesis of spherical hydroxyapatite nanoparticles and their in situ cytotoxicity study, Adv. Nano. Res. 4 (2016) 295.

[40] C. L. Popa, C. S. Ciobanu, S. L. Iconaru, M. Stan, A. Dinischiotu, C. C Negrila, M. Motelica-Heino, R. Guegan, D. Predoi, Systematic investigation and in vitro biocompatibility studies on mesoporous europium doped hydroxyapatite, Open Chem. 2014, 12(10) 1032-1046.

[41] R. Murugan, S. Ramakrishna, Production of ultra-fine bioresorbable carbonated hydroxyapatite, Acta Biomater. 2 (2006) 201-206.

[42] Veselinovic, L., Karanovic, L., Stojanovic, Z., Bracko, I., Markovic, S., Ignjatovic, N., Uskokovic, D. J. Appl. Crystallogr. 2010, 43, 320.

[43] T. A. R. M. Lima and M. E. G. Valerio, "X-ray absorption fine structure spectroscopy and photoluminescence study of multifunctional europium (III)doped hydroxyapatite in the presence of cationic surfactant medium," J. Lumin., vol. 201, no. Iii, pp. 70–76, 2018.

[44] J.C. Elliott, Structure and Chemistry of the Apatites and Other Calcium Orthophosphates, Elsevier Press, Amsterdam, 1994.

[45] T. Suzuki, T.Hatsushika, M.Miyake, Synthetic hydroxyapatites as inorganic cation exchangers. Part2 , J.Chem.Soc., FaradayTrans.178 (1982) 3605–3611.

[46] C. S. Ciobanu, C. L. Popa, D. Predoi, Sm:HAp Nanopowders Present Antibacterial Activity against Enterococcus faecalis, J. Nanomater., 2014, 2014, Article ID 780686.

[47] C. S. Ciobanu, S. L. Iconaru, M. C. Chifiriuc, A. Costescu, P. Le Coustumer, D. Predoi, Synthesis and Antimicrobial Activity of Silver-Doped Hydroxyapatite Nanoparticles, BioMed Res. Intern. 2013, 2013, Article ID 916218.

[48] A. Costescu, C. S. Ciobanu, S. L. Iconaru, R. V. Ghita, C. M. Chifiriuc, L. G. Marutescu, D. Predoi, Fabrication, Characterization, and Antimicrobial Activity, Evaluation of Low Silver Concentrations in Silver-Doped Hydroxyapatite Nanoparticles, J. Nanomater. 2013, 2013, Article ID 194854.

[49] C. S. Ciobanu, C. L. Popa, D. Predoi, Cerium doped hydroxyapatite nanoparticles synthesized by coprecipitation method, J. Serb. Chem. Soc. 2016, 81(4), 433-446.

[50] C. S. Ciobanu, S. L. Iconaru, F. Massuyeau, L. V. Constantin, A. Costescu, D. Predoi, Synthesis, Structure, and Luminescent Properties of Europium-Doped Hydroxyapatite Nanocrystalline Powders, J. Nanomater. 2012, 2012, Article ID 942801.